NANO LETTERS

Letter

pubs.acs.org/NanoLett

Linear-Grating Triboelectric Generator Based on Sliding Electrification

Guang Zhu,[†,§] Jun Chen,[†,§] Ying Liu,[†] Peng Bai,[†] Yu Sheng Zhou,[†] Qingshen Jing,[†] Caofeng Pan,[‡] and Zhong Lin Wang*[,†,‡]

[†]School of Materials Science and Engineering, Georgia Institute of Technology, Atlanta, Georgia 30332-0245, United States

[‡]Beijing Institute of Nanoenergy and Nanosystems, Chinese Academy of Sciences, China

Supporting Information

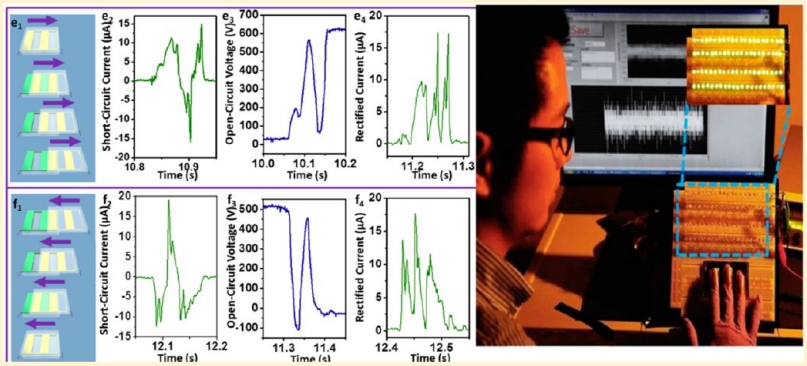

ABSTRACT: The triboelectric effect is known for many centuries and it is the cause of many charging phenomena. However, it has not been utilized for energy harvesting until very recently.[1−5] Here we developed a new principle of triboelectric generator (TEG) based on a fully contacted, sliding electrification process, which lays a fundamentally new mechanism for designing universal, high-performance TEGs to harvest diverse forms of mechanical energy in our daily life. Relative displacement between two sliding surfaces of opposite triboelectric polarities generates uncompensated surface triboelectric charges; the corresponding polarization created a voltage drop that results in a flow of induced electrons between electrodes. Grating of linear rows on the sliding surfaces enables substantial enhancements of total charges, output current, and current frequency. The TEG was demonstrated to be an efficient power source for simultaneously driving a number of small electronics. The principle established in this work can be applied to TEGs of different configurations that accommodate the needs of harvesting energy and/or sensing from diverse mechanical motions, such as contacted sliding, lateral translation, and rotation/rolling.

KEYWORDS: *Electrification, triboelectric generator, sliding, energy harvesting*

The triboelectric effect is a type of charge transfer by which two materials, after contact with each other, become electrically charged in opposite signs.[6−8] Most daily static electricity can be explained by the triboelectric effect. Though the fundamental mechanism of this effect is still under investigation,[9−15] it has been utilized in applications including electrostatic separations,[16] photocopying,[17] laser printing,[18] self-assembly,[19−26] and chemical systems.[27−30] Recently, this effect has been innovatively applied in energy harvesting to fabricate triboelectric generators (TEGs) that convert small-scale mechanical energy into electricity.[1−5] The TEG offers a new paradigm for simple, extremely low-cost, and scalable green energy technology. However, the previously demonstrated TEGs require periodic contact and separation of two materials that have opposite triboelectric polarities, making it only applicable to harvest energy from intermittent impact or shock. More critically, an indispensable design of the TEG is a cavity with constantly changing volume, which makes the TEG difficult for device packaging and largely limits its applications in atmospheres with high humidity, corrosive chemicals or gases, and in water or other liquids.

In this paper, we present a new principle of TEG that is based on sliding electrification between two surfaces, which overcomes the limitations of previous TEGs and greatly expands the applicability of the TEG for diverse forms of mechanical motions. Owing to the coupling between triboelectric effect and electrostatic effect, induced electrons form alternating current between electrodes as reciprocating sliding friction occurs. With linear grating introduced to the sliding surfaces, substantial enhancements of output charge, output current, and current frequency are achieved. At a sliding velocity of 10 m/s, a TEG (6.4 cm × 3.8 cm) with 10 grating units is equivalent to a continuous current source of 0.44 mA (corresponding current density of 0.18 A/m^2) at an open-circuit voltage of 615 V. The

Received: March 10, 2013
Revised: April 8, 2013
Published: April 11, 2013

dx.doi.org/10.1021/nl4008985 | *Nano Lett.* 2013, 13, 2282−2289

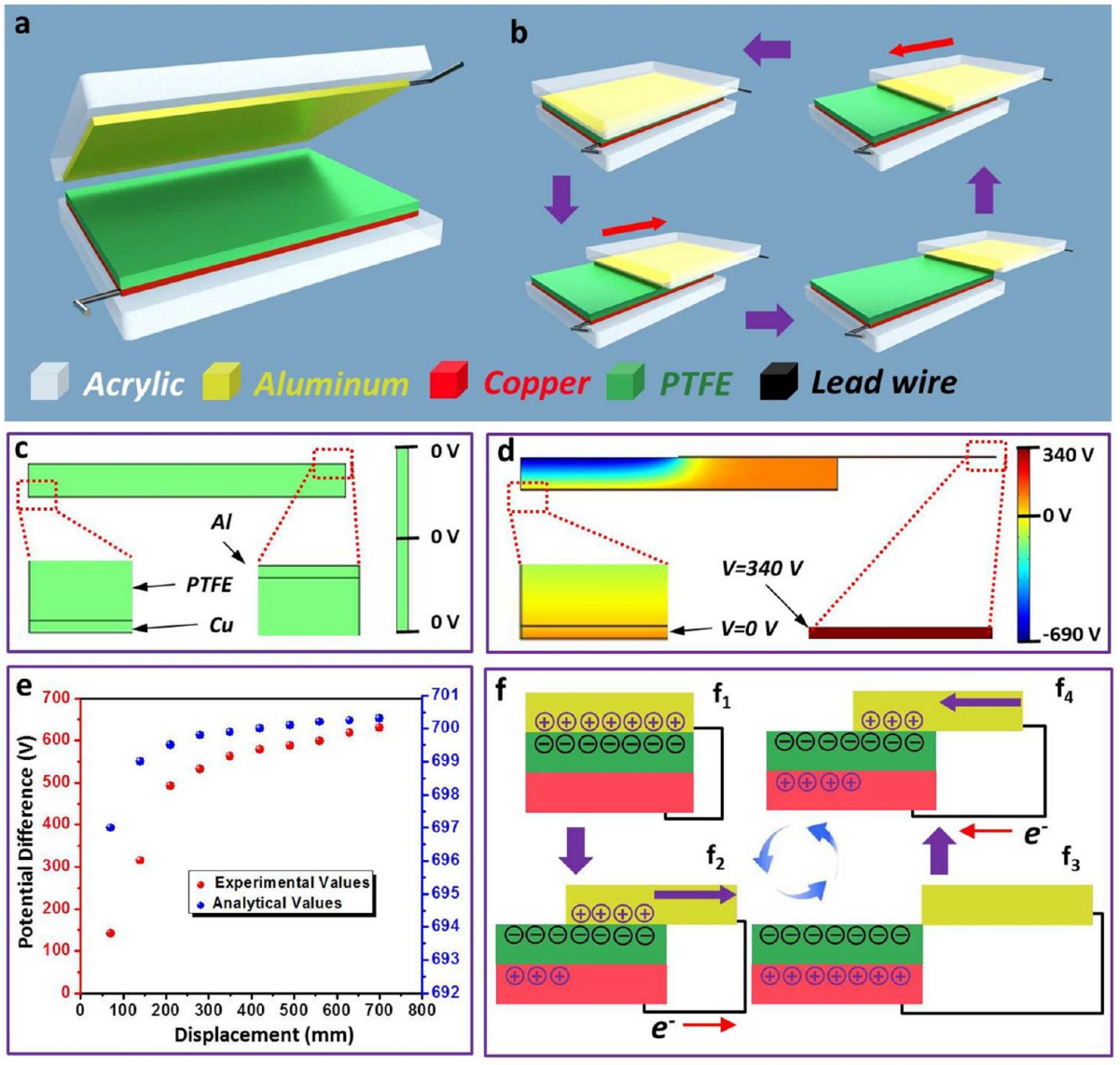

Figure 1. Triboelectric generator based on sliding electrification. (a) Schematic of a TEG without grating. The upper substrate is tilted to clearly demonstrate the structure. (b) A complete sliding cycle of the TEG at different percentage of plate mismatching areas. (c) COMSOL simulation result of electric potential distribution when the two surfaces are fully aligned without any displacement caused by sliding. (d) COMSOL simulation result of electric potential distribution when the two surfaces are halfway displaced. (e) Electric potential difference between the aluminum electrode and the copper electrode as a function of the displacement. Red dots and blue dots represent experimental values and analytical values, respectively. (f) A cycle of electricity generation process for illustrating the mechanism of the TEG: (f_1) fully aligned position, (f_2) the two surfaces are sliding apart, (f_3) fully displaced position, and (f_4) the two surfaces are sliding back together.

electric output is expected to be further greatly scaled up with finer grating. Driven by reciprocating tangential force from a human hand, the grating TEG was capable of simultaneously and continuously powering tens of commercial light-emitting diode (LED) bulbs. The principle demonstrated in this paper can be further applied to configurations other than planar surfaces, such as cylinders, tubes, and rotational discs, harvesting mechanical energy not just from translational motion but also from rotational/rolling motion. Therefore, this work establishes the fundamentals of a versatile solution to harvest diverse forms of mechanical energy, including rolling wheels, wind power, and water flow, provided that robust engineering design and packaging technology are available. The principle can also be used to design self-powered motion sensors for detecting translation or rotation.

The basic structure of the TEG is sketched in Figure 1a. It has a structure in which two contacting surfaces that can slide smoothly with one against the other. Acrylic was selected as a substrate material due to its decent strength, lightweight, and good machinability. On one substrate, aluminum thin film plays dual roles of an electrode and a sliding surface. On the other substrate, copper electrode is sandwiched between the substrate and a polytetrafluoroethylene (PTFE) film. The PTFE film acts as another sliding surface. The detailed fabrication process is discussed in Methods Summary. At original position, the two sliding surfaces are fully aligned with one sitting freely on the other. Driven by a tangential force applied to a substrate, relative displacement in contact mode occurs in lateral direction. After the two surfaces are fully displaced, the reciprocating force retraces them back to the aligned position (Figure 1b).

dx.doi.org/10.1021/nl4008985 | *Nano Lett.* 2013, 13, 2282−2289

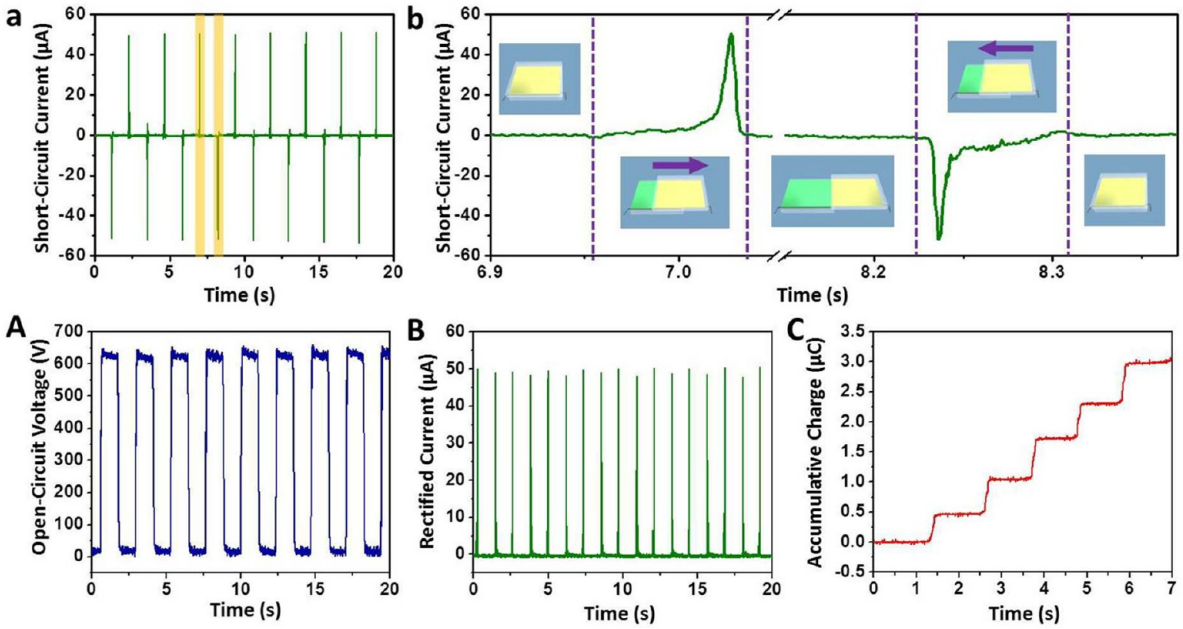

Figure 2. Electrical measurement results of a TEG without grating. (a,b) Short-circuit current (I_{sc}) (a) and enlarged view of a cycle (b) highlighted in (a). Insets: relative positions between the two sliding surfaces that correspond to the I_{sc} result. (c) Open-circuit voltage (V_{oc}). (d) Rectified current by a full-wave diode bridge. (e) Accumulative induced charges generated by the TEG. Each step represents a one-way sliding process across the entire length of the TEG. The diode bridge is used so that the induced charges can be added up. Note: The TEG has a size of 6.4 cm × 3.8 cm.

The principle of the TEG is explained by the coupling between triboelectric effect and electrostatic effect. Once the PTFE film is brought into contact with the aluminum thin film, surface charge transfer takes place due to the triboelectric effect or contact electrification. Because PTFE is much more triboelectrically negative than aluminum, electrons are injected from aluminum into PTFE. At aligned position, though triboelectric charges present on the surfaces, positive ones on aluminum are fully compensated by the negative ones on PTFE, producing no electric field in surrounding space if the electric field at the edge is ignored (Figure 1c). Once a relative displacement is introduced by an externally applied force in the direction parallel to the surfaces, triboelectric charges are not compensated at the displaced/mismatched areas, resulting in the creation of an effective dipole polarization parallel to the direction of the displacement. Therefore, the uncompensated charges generate electric potential difference (EPD) across the two electrodes, as illustrated by a simulation plot via COMSOL in Figure 1d. If electric potential of the copper electrode is set to be zero, the EDP can be analytically expressed as a function of the displacement under simplified approximations (see Supporting Information for detailed derivation of the analytical model)

$$\begin{aligned} EPD &= U_{Al} - U_{Cu} \\ &= \frac{q}{2\pi\varepsilon_0 WL}\int_0^t \tan^{-1}\left(\frac{l}{t}\right)dt \\ &= \frac{q}{2\pi\varepsilon_0 WL}\left[\frac{l}{2}\ln(t^2+l^2) + t\,\tan^{-1}\left(\frac{l}{t}\right)\right] \end{aligned} \quad (1)$$

where l is the mismatched displacement between the two sliding plates, q is the quantity of the triboelectric charges on one plate, ε_0 is the vacuum permittivity, L is the length of the TEG's plate, W is the width of the TEG, and t is the thickness of the PTFE film.

The EDP is essentially the open-circuit voltage (V_{oc}) that can be experimentally measured. The theoretical prediction on the V_{oc} from the analytical mode fits the trend of the experimental data (Figure 1e). These two sets of results both reveal that the V_{oc} drastically increases once the displacement occurs and quickly reaches a nearly saturated value. This observation can be derived from eq 1 on the condition that the sliding surface has lateral dimensions that are much larger than the PTFE's thickness ($L \gg t$, $W \gg t$). It is noticed in Figure 1e that the theoretical values saturate faster than the experimental values. It is likely to result from the simplifications made in the analytical derivation and nonideal factors in experiment such as rough sliding surfaces and thus inevitably created gap in between. Therefore, the actual separation between the electrodes along vertical direction during sliding may be much larger than the PTFE's thickness, making the experimental values saturate at a slower rate.

If the two electrodes are electrically connected, once displacement is established, the uncompensated negative triboelectric charges on PTFE will repulsively drive free electrons on the copper electrode to the aluminum electrode, neutralizing the positive triboelectric charges and leaving behind positive induced charges (Figure 1f$_2$). The flow of induced electrons lasts until the displacement reaches the maximum. On the basis of our assumptions made in the analytical model, the induced charges equal the triboelectric charges in quantity (see Supporting Information for details). Therefore, at fully displaced position, the positive triboelectric charges are completely balanced out by induced electrons (Figure 1f$_3$), indicating no more current flow. As the displacement is diminished by the reciprocating force, the induced electrons flow back to the copper electrode (Figure 1f$_4$) until the fully aligned position is restored (Figure 1f$_1$). Therefore,

dx.doi.org/10.1021/nl4008985 | Nano Lett. 2013, 13, 2282−2289

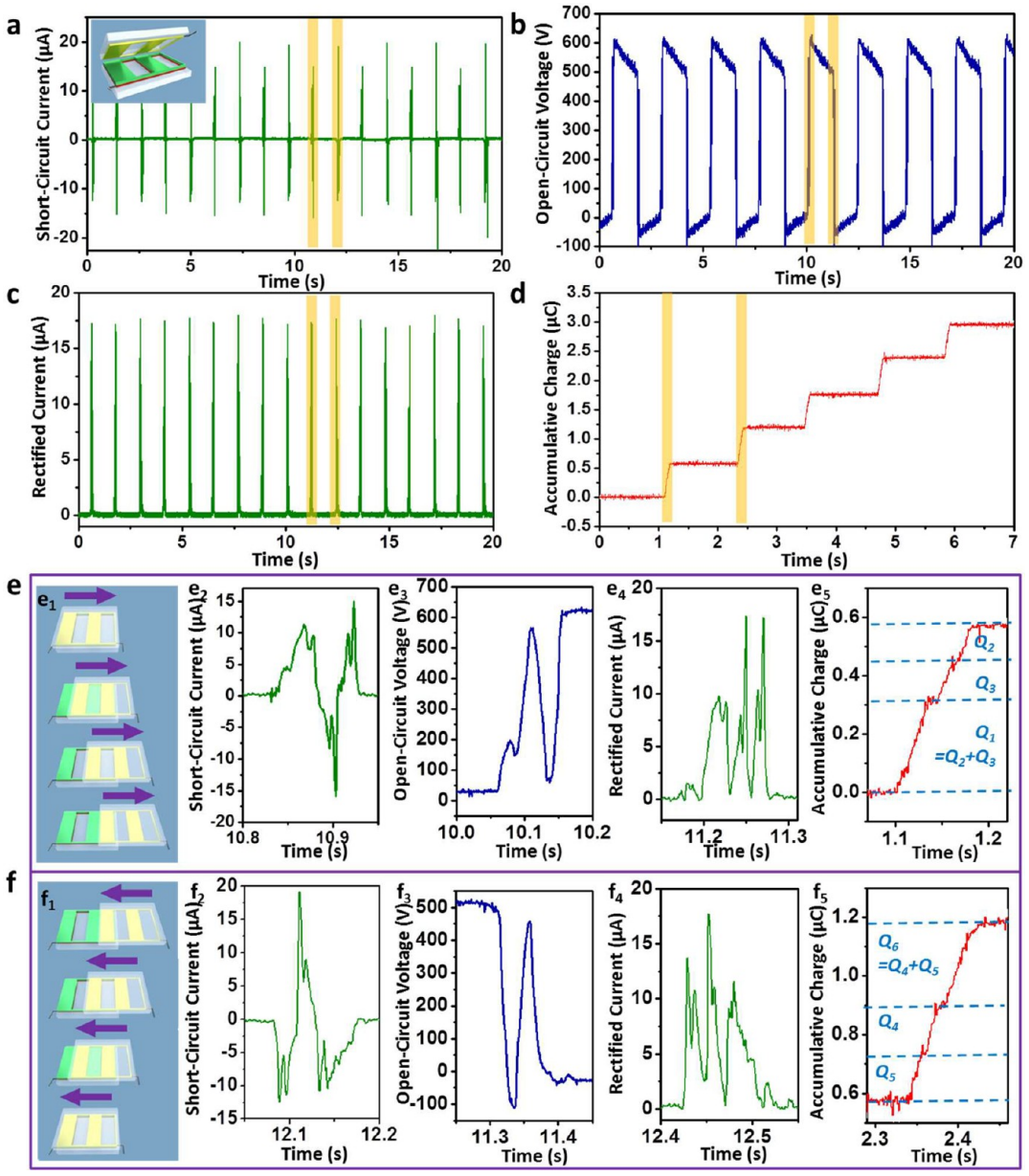

Figure 3. Electrical measurement results of a grating TEG with two grating units. (a,b) Short-circuit current (a) and open-circuit voltage (b) of the TEG. (c,d) Rectified current (c) and accumulative induced charges (d) generated by the TEN. (e) Electrical measurement results as the two surfaces are sliding apart: (e_1) different stages of the sliding process, (e_2) enlarged view of the I_{sc} in the first highlighted section in (a), (e_3) enlarged view of the V_{oc} in the first highlighted section in (b), (e_4) enlarged view of the rectified current in the first highlighted section in (c), and (e_5) enlarged view of the accumulative charges in the first highlighted section in (d). (f) Electrical measurement results as the two surfaces are sliding back together: (f_1) different stages of the sliding process, (f_2) enlarged view of the I_{sc} in the second highlighted section in (a), (f_3) enlarged view of the V_{oc} in the second highlighted section in (b), (f_4) enlarged view of the rectified current in the second highlighted section in (c), and (f_5) enlarged view of the accumulative charges in the second highlighted section in (d). Note: The TEG has a size of 6.4 cm × 3.8 cm with unit length of 1.6 cm.

in the entire process, alternating current (ac) is produced through the external load.

To characterize the performance of a TEG with a plate size of 6.4 cm × 3.8 cm, the short-circuit current (I_{sc}) and open-circuit voltage (V_{oc}) were measured at an average sliding velocity of 0.6 m/s introduced by a linear motor. As shown in Figure 2a, the I_{sc} exhibits peaks of alternating directions. An enlarged view of two adjacent peaks is displayed in Figure 2b. Increasing displacement gives a positive current peak, while shrinking displacement leads to a negative one. No electric current is produced at either aligned or entirely displaced position, as illustrated by insets in Figure 2b. The V_{oc} switches between zero and a maximum value, which corresponds to the aligned and fully displaced positions, respectively. The experimentally obtained results are fully consistent with the aforementioned theoretical analysis. Enabled by a full-wave diode bridge, the ac electric output can be rectified to a direct current (dc) signal (Figure 2d). With the diode bridge, the total accumulative induced charges, independent of sliding direction, can be added up. Demonstrated in Figure 2e, every step represents an output current resulting from a one-way sliding motion, generating 0.6 μC of induced charges on average. Correspondingly, the area density of the triboelectric charges is calculated to be 257 $\mu C/m^2$, which is consistent with previous reports.[3,5]

dx.doi.org/10.1021/nl4008985 | *Nano Lett.* 2013, 13, 2282−2289

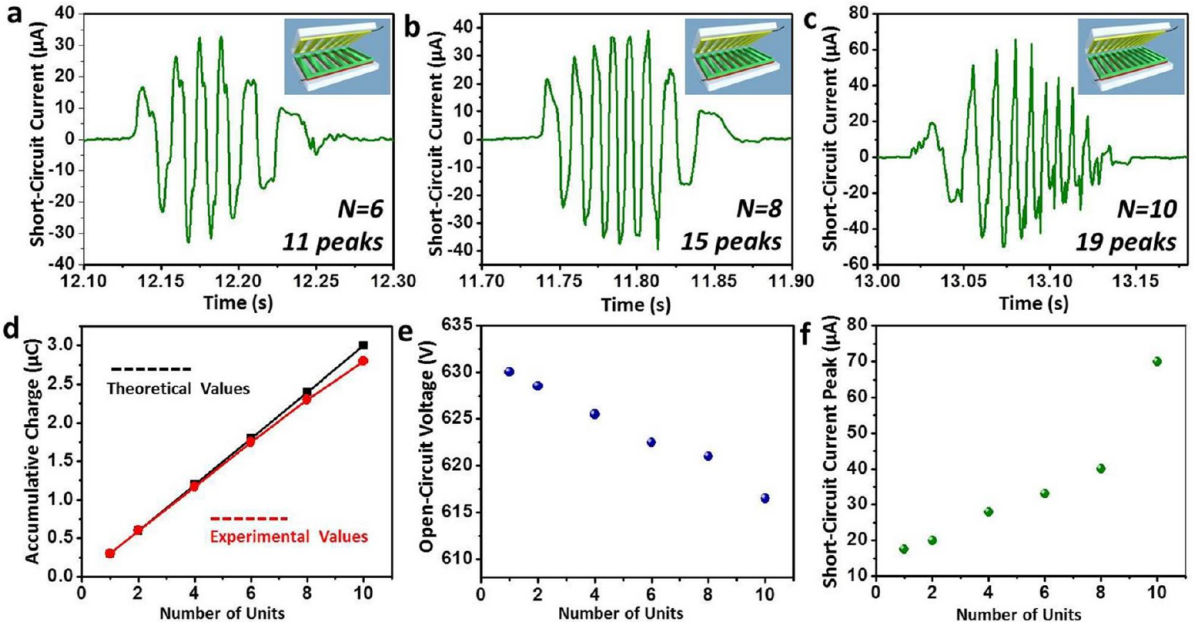

Figure 4. Electrical measurement results of grating TEGs with multiple grating units within a fixed total length. (a) Short-circuit current of a grating TEG with six grating units for a single sliding process across the full length of the TEG. Inset: schematic of the TEG structure. (b) Short-circuit current of a grating TEG with eight grating units for a single sliding process across the full length of the TEG. Inset: schematic of the TEG structure. (c) Short-circuit current of a grating TEG with 10 grating units for a single sliding process across the full length of the TEG. Inset: schematic of the TEG structure. (d) Accumulative induced charges generated for a single sliding process across the full length of a TEG as a function of grating units. (e) Open-circuit voltage as a function of grating units. (f) Maximum values of short-circuit current as a function of grating units.

Introducing linear grating on the sliding surfaces enables the new principle to become an extremely efficient means for energy harvesting, and it is far superior to the previously demonstrated ones in total output charge, current frequency, and efficiency.[1−5] Linear grating with uniform period is fabricated on both sliding surfaces. The rows of grating units have the same size as intervals in between with all rows being electrically connected at both ends by two buses. The grating patterns on both sliding surfaces are identical so that they can match well with each other when aligned. The detailed fabrication process is presented in Methods Summary and Supporting Information Figure S2. Although the grating design reduces the total contact area by half thus seemingly sacrifices half of the triboelectric charges, it increases the percentage of the mismatched area to 100% for a displacement of only a grating unit length rather than the entire length of the TEG so that it dramatically increases the transport efficiency of the induced charges. Induced free electrons can be pumped back and forth between electrodes for multiple times due to the grating structure, providing multifolds of output charge compared to a nongrating TEG. Every row of the grating units can be considered as a reduced-sized TEG; it is in parallel connection with all other rows through buses. In contrast to a nongrating TEG that needs to be fully displaced in order to complete pumping of the induced charges for one time, the grating TEG only requires a displacement of a unit length to completely transport the induced charges, largely improving the energy conversion efficiency. With further displacement of another length of the unit, back flow of the induced charges can be realized. Therefore, for a one-way sliding process across the whole length of the TEG, the induced charges can be pumped for $(2N-1)$ times in total, where N is the number of grating units. If we take into account that the contacting area decreases as the two surfaces slide apart, the following equation represents the total induced charges Q that the grating TEG can provide for a single sliding across the entire length of the TEG

$$\begin{aligned} Q &= Nq' + |-q' \times (N-1)| + q' \times (N-1) \\ &\quad + \cdots + |-q'| + q' \\ &= Nq' + 2q' \times \sum_{i=1}^{N-1} i \\ &= \frac{(2q'N)N}{2} \end{aligned} \tag{2}$$

where q' is the induced charges generated from a single grating unit for a displacement of the unit length (see Supporting Information for detailed illustration).

The total maximum induced charges generated by a nongrating TEG can be equivalently expressed as $2q'N$ (Supporting Information). Therefore, eq 2 indicates that the total induced charges linearly increase with the grating density. To validate the above analysis, electrical measurement was performed on a grating TEG that has two units (inset in Figure 3a) with unit length of 1.6 cm. Results of I_{sc}, V_{oc}, rectified current, and accumulative charges are presented in Figure 3a−d, respectively. Figure 3e displays the measured results in a sliding process from aligned position to a fully displaced position. The I_{sc} for the grating TEG exhibits alternating direction, producing a total of three current peaks (Figure $3e_2$). It indicates that the induced electrons are pumped back and forth between electrodes for three times. Correspondingly, the V_{oc} oscillates between zero and the maximum value also for three times (Figure $3e_3$). By a diode bridge, all of the three current peaks are completely rectified (Figure $3e_4$), leading to accumulative induced charges that can be added up (Figure $3e_5$). Close inspection on Figure $3e_2$ and Figure $3e_5$ reveals that the first current peak delivers twice as

dx.doi.org/10.1021/nl4008985 | Nano Lett. 2013, 13, 2282−2289

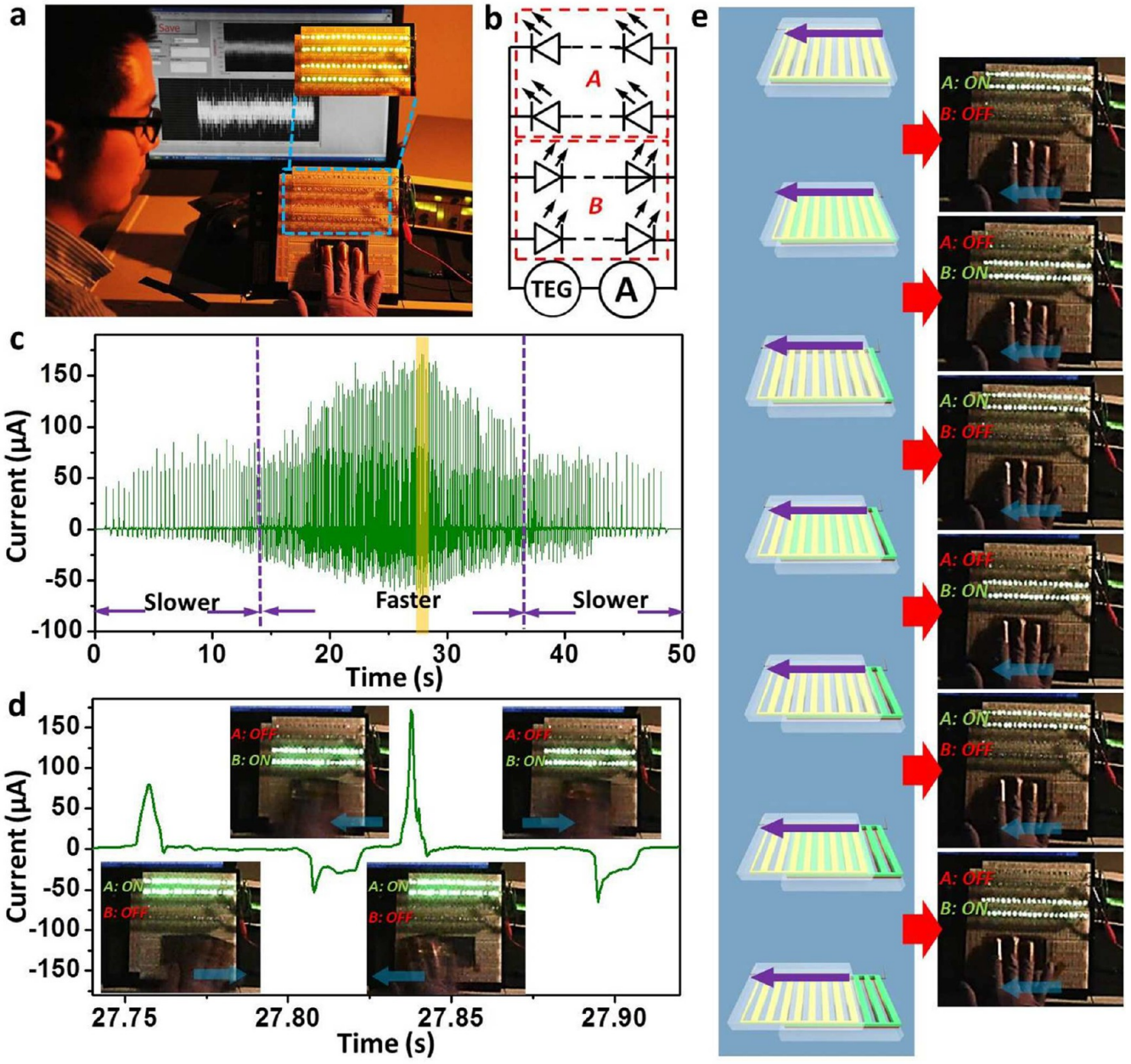

Figure 5. Demonstration of the TEG as a direct power source for driving conventional electronics. (a) Photograph that shows the experimental setup. Inset: four rows of LED bulbs that are being lighted up. (b) Electric circuit diagram, indicating the four rows of LEDs that are divided into two groups with reversed connection polarities. (c) Short-circuit current generated from a nongrating TEG as the relative displacement results from reciprocating sweeping of a human hand. (d) Enlarged view of the section highlighted in (c). Insets: Snapshots that show the states of the two groups of LEDs corresponding to the current peaks. (e) Different stages of the sliding process as a TEG with eight grating units is being slid apart (left column) and corresponding states of the two groups of LEDs during the sliding process (right column).

much charge quantity as the second and the third peaks. This observation is correctly predicted by eq 2. The total induced charges provided by all of the three current peaks reach approximately 0.6 μC. This quantity equals that from a nongrating TEG, which is consistent with eq 2. If sliding direction is reversed as indicated in Figure 3f, measurement results are also reversed in both polarity and sequence.

Experimental data from grating TEGs with more units further confirm the validity of our theoretical analysis. For a single sliding process, the I_{sc} data produced by grating TEGs having 6, 8, and 10 units are presented in Figure 4a–c, corresponding to a unit length of 0.5, 0.4 and 0.3 cm, respectively, with a constant full length of the TEG (6.4 cm). The total counts of ac peaks are in accordance with eq 2. The resemblance of the current peaks to a wave packet is explained in the Supporting Information. The enhancement of charge output by the grating structure is plotted in Figure 4d. With 10 grating units, a total of 2.8 μC of induced charges can be generated within 6.4 ms at a sliding velocity of 10 m/s, which is equivalent to a continuous dc source of 0.44 mA. Ideally, according to eq 2, the total induced charges are proportional to the density of the grating units. If the grating size is further scaled down to 30 μm, an ideal enhancement of another 100 times is expected, making the TEG comparable to various types of solar cells in output current and in current

dx.doi.org/10.1021/nl4008985 | *Nano Lett.* 2013, 13, 2282–2289

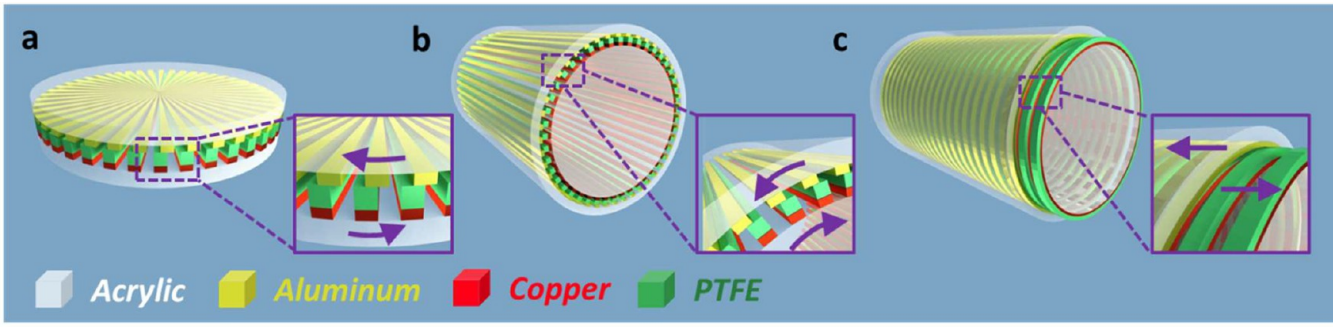

Figure 6. Different configurations of grating TEGs in which the principle of sliding electrification can be applied. (a) Two concentric discs that can harvest energy from rotation. Inset: enlarged view that shows the rotational directions. (b) Two coaxial rubes that can harvest energy from rolling. Inset: enlarged view that shows the rolling directions. (c) Two coaxial rubes that can harvest energy from linear piston motion. Inset: enlarged view that shows the moving directions.

density.[31−33] An estimation for the N = 10 gives an output conversion efficiency of ∼8−31% (Supporting Information).

Though the experimental data closely match the theoretical values for $N \leq 4$, slight deviation starts to appear if N further increases (Figure 4d). The deviation may be attributed to two probable reasons. The first is nonideal orientation mismatch. The two sliding surfaces are likely to have an angle of mismatch that is introduced by experimental operation (Supporting Information Figure S5). As the length of the grating units shrinks, the angle of mismatch will exert more substantial effect on the effective contact area between the two surfaces, leading to increasingly reduced output charge (see Supporting Information for detailed analysis). This effect can be largely eliminated by more precise alignment during experiment operation. Second, we suggest that assumptions made in the analytical theory may become imprecise for very fine grating units due to the edge effect of each unit. The assumption of infinite charged plane will no longer hold once the grating edges can dominantly affect the electric field distribution, leading to reduced quantity of induced charges. Further systematic investigation by both experiment and simulation is required to quantitatively understand this nonideal effect. As diagramed in Figure 4e, the V_{oc} is only weakly related to the number of grating units, though slight reduction can be observed. The reduction can also be attributed to the increasingly stronger effect from the mismatched angle. Besides, as revealed in eq 1, finer grating units will theoretically give a smaller V_{oc}, though this effect may be dominant only when the grating unit has a length approaching the PTFE's thickness. The advantages of the grating structure include not only the enhanced total transported charges but also improved output current. With constant sliding velocity, finer grating shortens the time to transport induced charges between the electrodes for one time, resulting in higher output current (Figure 4f). However, the peak of I_{sc} does not increase linearly with the number of units, which may result from nonuniform velocity during sliding process.

To demonstrate the capability of the new principle as a direct power source, a total of 80 commercial LED bulbs were utilized as operating load (Figure 5a). They were divided into two groups, which were connected to a TEG with reversed polarity in order to clearly demonstrate the ac output without rectification (Figure 5b). Shown in Figure 5a, one substrate of the TEG was fixed on a breadboard where the LEDs were installed, while the other one was attached to human fingers. As the hand swept back and forth, the sliding was realized. For a nongrating TEG, the output current it delivers to the load is displayed in Figure 5c. It is noticed that faster sweeping generates higher current peaks as compared with those from slower sweeping. Every current peak was capable of simultaneously lighting up one group of LEDs (see Supporting Information Movie 1). Because of the ac output, the two LED groups were alternately lighted up, as indicated by "ON" and "OFF" states in Figure 5d. It is worth noticing that a single sliding process corresponds to only a single current peak, which is visualized by snapshots in Figure 5d. In comparison, a grating TEG is able to power the load for multiple times within a single sliding. For a TEG with eight grating units, only a displacement of a unit length was required to light up the LEDs. Therefore, with grating structure, not only can the TEG have substantial enhancements of current and charges, but also it can provide high frequency ac output that enables continuous operation of electric devices (see Supporting Information Movies 2 and 3).

The principles demonstrated for the grating TEG can be applied to other configurations (Figure 6), greatly extending the practicability of this technology. Besides the planar design, other configurations include, but are not limited to, concentric discs having relative rotation (Figure 6a) and coaxial tubes having rotational motion (Figure 6b) and piston motion (Figure 6c). With these diverse designs, no matter whether the triggering force is intermittent impact or continual press, the sliding electrification principle of the TEG becomes a universal solution to harvesting multiple forms of ambient mechanical energy, including translation, rotation/rolling.

In summary, we invented a new principle of grating TEG based on sliding electrification. The sliding between the two contact surfaces leads to uncompensated triboelectric charges on displaced areas, which drive induced charges between electrodes. Linear grating enables substantial enhancements of output charge, output current, and current frequency. With 10 grating units that are 3 mm in length for each, the TEG is effectively equivalent to a continuous dc source of 0.44 mA (corresponding current density of 0.18 A/m^2), and an energy conversion efficiency of 8−31% has been demonstrated. Finer grating units can further greatly boost up the electric output, though nonlinear effect needs to be investigated in order to achieve optimal design. Powered by the grating TEG that produces high-frequency ac output, tens of commercial LED bulbs were simultaneously and continuously lighted up. The basic concept and design demonstrated in this work can be extended to other configurations that are applicable to harvest multiple forms of ambient mechanical energy. Therefore, this work lays a fundamental groundwork for a versatile solution to harvesting diverse forms of mechanical energy, including rolling wheels,

dx.doi.org/10.1021/nl4008985 | *Nano Lett.* 2013, 13, 2282−2289

wind power, and water flow. Furthermore, the demonstrated principle can also be used to design self-powered motion sensors (active sensors) for detecting translation or rotational motions.

Methods Summary. *Fabrication of the Nongrating TEG.* Two acrylic substrates with a size of 6.4 cm × 3.8 cm × 0.16 cm were prepared by laser cutter. On one of the substrate, aluminum layer with a thickness of 100 nm was deposited by e-beam evaporator. On a PTFE film with a thickness of 100 μm, a copper electrode was prepared by depositing 100 nm of copper. Then, the copper-coated PTFE was adhered to the other substrate with the uncoated surface on the top. PDMS (ratio of base and curing agent: 20 to 1) can be used as the adhesion layer between the PTFE film and the substrate. The PDMS can substantially reduce the fluctuation of the grating structure height by smoothing roughness and curvature of the substrate. Finally, the two substrates were brought together with the aluminum contacting the uncoated PTFE. Lead wires were connected to the two metal electrodes for measurement.

Fabrication of the Grating TEG. The fabrication process of the grating TEG is illustrated in Supporting Information Figure S2. Two acrylic substrates with a size of 6.4 cm × 3.8 cm × 0.16 cm were prepared by laser cutter. Two identical sets of masks for the grating pattern were also fabricated from acrylic by the laser cutter. One mask was mounted onto a substrate, while the other one was mounted onto the PTFE film. Then aluminum and copper were deposited through the open window areas of the masks onto the substrate and the PTFE film, respectively. After deposition, the masks were removed. The copper-coated PTFE was adhered to the other substrate with the uncoated surface on the top. Grating structure was created on the PTFE surface by cutting off the area that has no copper coating on the other side. Finally, the two substrates were brought together with the aluminum contacting the uncoated PTFE. Metal wires were connected to the two metal electrodes for measurement.

■ ASSOCIATED CONTENT

Supporting Information

More detailed information about grating TEG fabrication, analytical model for calculating the open-circuit voltage of the TEG, the effect of misorientation angle estimation, as well as energy conversion efficiency estimation. This material is available free of charge via the Internet at http://pubs.acs.org.

■ AUTHOR INFORMATION

Corresponding Author

*E-mail: zlwang@gatech.edu.

Author Contributions

§G.Z and J.C. contributed equally to this work.

Notes

The authors declare no competing financial interest.

■ ACKNOWLEDGMENTS

Research was supported by Airforce, U.S. Department of Energy, Office of Basic Energy Sciences (Award DE-FG02-07ER46394), NSF (0946418), and the Knowledge Innovation Program of the Chinese Academy of Science (Grant KJCX2-YW-M13). Patents have been filed based on the research results presented in this manuscript.

■ REFERENCES

(1) Fan, F. R.; Tian, Z. Q.; Wang, Z. L. *Nano Energy* **2012**, *1*, 328−334.
(2) Fan, F. R.; Lin, L.; Zhu, G.; Wu, W. Z.; Zhang, R.; Wang, Z. L. *Nano Lett.* **2012**, *12*, 3109−3114.
(3) Zhu, G.; Pan, C. F.; Guo, W. X.; Chen, C. Y.; Zhou, Y. S.; Yu, R. M.; Wang, Z. L. *Nano Lett.* **2012**, *12*, 4960−4965.
(4) Wang, S. H.; Lin, L.; Wang, Z. L. *Nano Lett.* **2012**, *12*, 6339−6346.
(5) Zhu, G.; Lin, Z. H.; Jing, Q. S.; Bai, P.; Pan, C. F.; Yang, Y.; Zhou, Y. S.; Wang, Z. L. *Nano Lett.* **2013**, *13*, 847−853.
(6) Lowell, J.; Rose-Innes, A. C. *Adv. Phys.* **1980**, *29*, 947−1023.
(7) Horn, R. G.; Smith, D. T. *Science* **1992**, *256*, 362−364.
(8) Horn, R. G.; Smith, D. T.; Grabbe, A. *Nature* **1993**, *366*, 442−443.
(9) Diaz, A. F.; Guay, J. *IBM J. Res. Dev.* **1993**, *37*, 249−259.
(10) Davies, D. K. *J. Phys. D: Appl. Phys.* **1969**, *2*, 1533−1537.
(11) Duke, C. B. *J. Appl. Phys.* **1978**, *49*, 315−321.
(12) Wiles, J. A.; Grzybowski, B. A.; Winkleman, A.; Whitesides, G. M. *Anal. Chem.* **2003**, *75*, 4859−4867.
(13) McCarty, L. S.; Winkleman, A.; Whitesides, G. M. *J. Am. Chem. Soc.* **2007**, *129*, 4075−4088.
(14) McCarty, L. S.; Whitesides, G. M. *Angew. Chem., Int. Ed.* **2008**, *47*, 2188−2207.
(15) Soh, S.; Kwok, S. W.; Liu, H.; Whitesides, G. M. *J. Am. Chem. Soc.* **2012**, *134*, 20151−20159.
(16) Kwetkus, B. A. *Part. Sci. Technol.* **1998**, *16*, 55−67.
(17) Schein, L. B. *Electrophotography and Development Physics*; Laplacian Press: Morgan Hill, CA, 1996.
(18) Pai, D. M.; Springett, B. E. *Rev. Mod. Phys.* **1993**, *65*, 163−211.
(19) Grzybowski, B. A.; Winkleman, A.; Wiles, J. A.; Brumer, Y.; Whitesides, G. M. *Nat. Mater.* **2003**, *2*, 241−245.
(20) Grzybowski, B. A.; Wiles, J. A.; Whitesides, G. M. *Phys. Rev. Lett.* **2003**, *90*, 083903−1−4.
(21) Kumar, A.; Pattarkine, M.; Bhadbhade, M.; Mandale, A. B.; Ganesh, K. N.; Datar, S. S.; Dharmadhikari, C. V.; Sastry, M. *Adv. Mater.* **2001**, *13*, 341−344.
(22) Tien, J.; Terfort, A.; Whitesides, G. M. *Langmuir* **1997**, *13*, 5349−5355.
(23) Caruso, F.; Lichtenfeld, H.; Giersig, M.; Mohwald, H. *J. Am. Chem. Soc.* **1998**, *120*, 8523−8524.
(24) Kalsin, A. M.; Fialkowski, M.; Paszewski, M.; Smoukov, S. K.; Bishop, K. J. M.; Grzybowski, B. A. *Science* **2006**, *312*, 420−424.
(25) Bishop, K. J. M.; Grzybowski, B. A. *ChemPhysChem.* **2007**, *8*, 2171−2176.
(26) Kalsin, A. M.; Grzybowski, B. A. *Nano Lett.* **2007**, *7*, 1018−1021.
(27) Liu, C.-Y.; Bard, A. J. *Nat. Mater.* **2008**, *7*, 505−509.
(28) Liu, C.-Y.; Bard, A. J. *J. Am. Chem. Soc.* **2009**, *131*, 6397−6401.
(29) Liu, C.-Y.; Bard, A. J. *J. Chem. Phys. Lett.* **2010**, *485*, 231−234.
(30) Baytekin, B.; Baytekin, H. T.; Grzybowski, B. A. *J. Am. Chem. Soc.* **2012**, *134*, 7223−7226.
(31) Law, M.; Greene, L. E.; Johnson, J. C.; Saykally, R.; Yang, P. D. *Nat. Mater.* **2005**, *4*, 455−459.
(32) Brabec, C. J.; Sariciftci, N. S.; Hummelen, J. C. *Adv. Funct. Mater.* **2001**, *11*, 15−26.
(33) Huynh, W. U.; Dittmer, J. J.; Alivisatos, A. P. *Science* **2002**, *295*, 2425−2427.